NANO LETTERS

Letter

pubs.acs.org/NanoLett

Stretchable and Transparent Electrodes using Hybrid Structures of Graphene–Metal Nanotrough Networks with High Performances and Ultimate Uniformity

Byeong Wan An,[†] Byung Gwan Hyun,[†] So-Yun Kim,[†] Minji Kim,[†] Mi-Sun Lee,[†] Kyongsoo Lee,[†] Jae Bon Koo,[§] Hye Yong Chu,[§] Byeong-Soo Bae,[¶] and Jang-Ung Park*[,†,‡]

[†]School of Materials Science and Engineering, Wearable Electronics Research Group, Low-Dimensional Carbon Materials Research Center and [‡]School of Energy and Chemical Engineering, Ulsan National Institute of Science and Technology (UNIST), Ulsan Metropolitan City, 689-798, Republic of Korea

[§]Components and Materials Research Laboratory, ETRI, Daejeon Metropolitan, 305-700, Republic of Korea

[¶]Department of Materials Science and Engineering, Korea Advanced Institute of Science and Technology (KAIST), Daejeon Metropolitan 305-701, Republic of Korea

S *Supporting Information*

ABSTRACT: Transparent electrodes that can maintain their electrical and optical properties stably against large mechanical deformations are essential in numerous applications of flexible and wearable electronics. In this paper, we report a comprehensive analysis of the electrical, optical, and mechanical properties of hybrid nanostructures based on graphene and metal nanotrough networks as stretchable and transparent electrodes. Compared to the single material of graphene or the nanotrough, the formation of this hybrid can improve the uniformity of sheet resistance significantly, that is, a very low sheet resistance (1 Ω/sq) with a standard deviation of less than ±0.1 Ω/sq, high transparency (91% in the visible light regime), and superb stretchability (80% in tensile strain). The successful demonstration of skin-attachable, flexible, and transparent arrays of oxide semiconductor transistors fabricated using hybrid electrodes suggests substantial promise for the next generation of electronic devices.

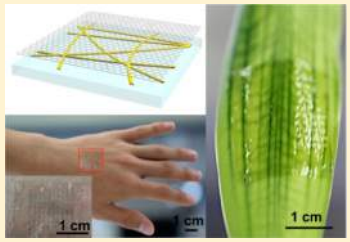

KEYWORDS: *Metal nanotrough, graphene, hybrid, transparent electrodes, stretchable electronics*

Transparent electrodes are an essential component in numerous electronic devices, such as displays, solar cells, touch screens, and light-emitting devices. In recent years, the fast-emerging fields of flexible and wearable electronics has created an urgent need for radically new form factors for those devices, including encoding mechanical flexibility and stretchability into transparent electrodes. Although indium tin oxide (ITO) is the material that is most commonly used for transparent electrodes, its use for applications in flexible and wearable electronics has been limited due to its brittleness and the scarcity of indium. Several alternatives to ITO, including conducting polymers,[1] carbon nanotubes,[1−5] graphene,[6−16] nanowires,[2,17−26] metal meshes,[15,27,28] and metal nanotrough networks[29] have been studied extensively for this purpose. Among these alternative materials, percolating networks of the one-dimensional (1D) metal nanotroughs have provided the lowest levels of sheet resistance (R_s), that is, less than 17 Ω/sq for transmittance (T) of >90%. Furthermore, their free-standing, mesh-like structures present good mechanical flexibility under both bending and stretching stresses (50% in bending or stretching strain). For the fabrication of such electrodes, electrospinning is used to produce free-standing, continuous nanofiber webs of polymers as a template to form the nanotrough by depositing metals onto the sacrificial template and then dissolving it selectively. Charge transport in the nanotrough occurs along the 1D metal pathways, and the ultralong geometries of the electrospun fibers facilitate the reduction of R_s by minimizing the number of junctions between the metal lines. Also, open spaces in the meshlike structures provide optical transparency. However, the nanotrough has several disadvantages, such as (i) a lack of uniformity of R_s due to the randomly distributed, nonuniform pitches of the electrospinning-related and metal nanotrough networks; (ii) difficulty in producing large-area nanotrough films over wafer scales; (iii) high contact resistance between the electrode and the active materials because of the nonconductive, large open spaces (>∼50 μm) within the networks; (iv) the significant increase of R_s that occurs when the size of the electrode pattern is decreased (related to its percolating properties); and (v) instability of the material in harsh environments. These disadvantages can limit the potential integration of nanotroughs into commercial devices.

Another promising alternative to ITO is two-dimensional (2D) graphene. Monolayer graphene can be distorted up to a strain of 4%[14] and still have a T of 97.7% (Supporting

Received: July 20, 2014
Revised: September 13, 2014
Published: October 9, 2014

   dx.doi.org/10.1021/nl502755y | *Nano Lett.* 2014, 14, 6322−6328

Information Figure 1) in the visible light range.[7] Despite graphene's high mechanical flexibility and good optical transparency, the R_s of undoped, synthesized graphene (>~ 250 Ω/sq) is much bigger than the R_s of ITO (<~80 Ω/sq with a T of ~90% at 550 nm).[6,11−13] For example, scalable graphene synthesis methods, such as chemical vapor deposition (CVD)[6,10−12] and epitaxial growth using silicon carbide,[9] generate polycrystalline graphene structures with defects, such as ripples, wrinkles, grain boundaries, folds, and cracks. These defects degrade the electric performance of graphene significantly. Although chemical doping methods[14,16] can decrease the R_s of graphene further, the instability of the graphene-dopant interactions shortens the lifetime of this doping effect and hence causes a time-variant increase of R_s.[15]

Herein, we report graphene−metal nanotrough hybrid structures as stretchable and transparent electrodes that provide high performance. The hybridization of metal nanowires (rather than nanotroughs) with graphene was explored in recent research.[30−32] However, to the best of our knowledge the hybrid formation using graphene and nanotroughs has not been assessed to determine its potential for enhancing the functionalities of transparent electrodes or to fabricate wearable electronic devices. In our approach, 1D, long networks of nanotroughs were integrated into 2D graphene without significant reduction of T. Both the conducting components of the nanotrough networks and the graphene allow simultaneous charge transport in this hybrid geometry, each complementing the disadvantages of the other component. This electrode can reduce R_s to as little as 1 Ω/sq for a T of 91% while preserving these electric and optical properties reliably under long-term thermal loadings. In addition, the formation of this hybrid improves its uniformity significantly, resulting in standard deviations of R_s that are only about 10% of those in the case of a nanotrough made of a single material. Also, the hybrid electrode has superb mechanical flexibility (folding with minimum bending radius of ~50 μm) and stretchability (maximum stretching strain of 50%). An example of the application of such a hybrid electrode is its use to fabricate flexible and transparent oxide semiconductor transistor arrays with the hybrid electrode serving as source/drain and interconnects. Furthermore, these arrays of devices can be attached to various nonplanar substrates, including the surfaces of eyeglasses, leaves, and human skin, suggesting promise for their use in the future in flexible and wearable electronic devices.

This hybrid conductive film can be formed simply by transferring a CVD-synthesized graphene layer onto the nanotrough, and the graphene is attached to the surface of the metal by van der Waals forces. As described in the previous work on the fabrication of the nanotrough,[33] free-standing nanofiber webs of a poly(vinyl alcohol) (PVA) polymer were produced (fiber diameter: ~1.8 μm) on a collector by electrospinning (Figure 1a). After directional deposition of metals (100 nm of Au) onto the upper side of the free-standing fibers, the lower surface (polymer side) of the fiber, where the metal was uncoated, was placed in contact with the desired substrate. Then, removing the polymeric sacrificial template using acetone, isopropyl alcohol (IPA), and deionized water (acetone for 10 min, followed by IPA and DI water in the volumetric ratio of 1:1 for 30 min) left only the nanotrough with a thin, convex, half-shell cross-section on the substrate. Figure 1a shows that transferring a CVD graphene layer onto the round surface of the nanotrough completed the fabrication

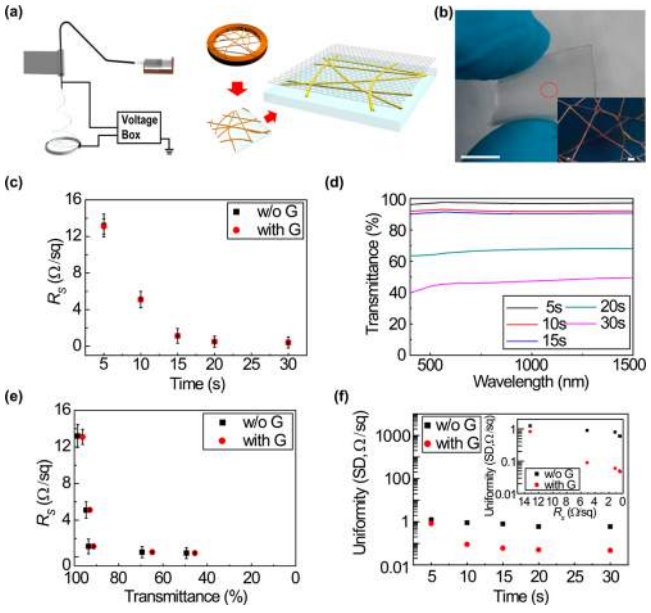

Figure 1. Fabrication processes, optical and electric properties of graphene−metal nanotrough hybrid structure. (a) Schematic images on the processes to form the graphene−metal nanotrough hybrid electrode. (b) Photograph of graphene−metal nanotrough hybrid film on a PDMS substrate. The scale bar indicates 2 cm. A magnified, optical micrograph of the hybrid is shown on the inset (scale bar; 10 μm). (c) Sheet resistance (R_s) of metal nanotrough or the hybrid as a function of spinning time. (d) Optical transmittance (T) spectra of the hybrid films fabricated with different spinning time. (e) T versus R_s of the hybrid. (f) The R_s uniformities (standard deviations, log-scale plots) of the nanotrough or the hybrid fabricated with diverse spinning time. A graph on the relationship between the uniformity and R_s is presented as an inset.

of the graphene−metal nanotrough hybrid structure with the generation of negligible cracks at the interfaces between the two components. (Supporting Information Figure 2) Figure 1b presents a photograph and an optical micrograph of this hybrid film on poly(dimethylsiloxane) (PDMS) as the substrate. Figure 1c shows the R_s of the hybrid electrodes as a function of the electrospinning time. Longer electrospinning time results in denser networks of the metal lines in the hybrid structure, thereby reducing the R_s of the hybrid below 1 Ω/sq. T also decreases as the electrospinning time increases due to more extensive coverage of the metal in the hybrid (Figure 1d, Supporting Information Figure 3). Only ~2−3% loss of T is introduced by the addition of graphene onto the nanotrough to form the hybrid material (Figure 1e). The T of the hybrid is almost consistent in the broad wavelength range from 400 to 1500 nm (Figure 1d). In contrast to the ITO, which represents strong absorption in the near-infrared regime,[22,33] the wideband flat spectra of this hybrid are highly desirable for many optoelectronic applications because they can enhance the efficiency of solar cells by using the near-infrared solar spectrum and also enable the use of the devices as near-infrared sensors and detectors.[29] Figure 1e shows plots of the R_s of the hybrid electrode with T at 550 nm. The hybrid demonstrated the superb performance as the transparent electrode, that is, 1.1 Ω/sq at T = 91% (for 15 s of electrospinning time). This optoelectronic property is superior to those of other transparent conducting materials, such as conducting polymers, graphene, carbon-nanotubes, metal grids, silver nanowire networks, copper nanowire networks, and ITO.[14,21,26,34−40]

dx.doi.org/10.1021/nl502755y | Nano Lett. 2014, 14, 6322−6328

Increasing the electrospinning time above ~20 s caused further reduction in R_s below 1 Ω/sq and relatively low T of less than ~70%.

Figure 1f indicates the uniformity of the R_s of the hybrid nanostructure compared to the single-material case of the nanotrough. The mean R_s and the standard deviation (SD) values in Figure 1c,f were measured at 30 different points of each sample. The mean R_s values of the singular metal nanotrough and its hybrid with graphene were very similar, as shown in Figure 1c, indicating that the nanotrough networks provide the main conductive pathways of charges with graphene acting as an additional component in the hybrid structure. Although the role of graphene in the reduction of R_s was insignificant, the graphene enhanced the uniformity of the hybrid remarkably. In the case of the nanotrough alone, randomly distributed, nonuniform pitches between the metal lines and the local disconnections of metals caused relatively large deviations in R_s. For example, the mean R_s and SD values of the nanotrough had almost the same order of magnitude (Figure 1f). However, in the hybrid structure, graphene occupies empty spaces in the nanotrough networks, thereby allowing charge transport across the metal networks, which can improve the uniformity significantly. Figure 1f indicates that this hybrid formation reduced the deviations of R_s by about 92% compared to the SD of the nanotrough alone.

The electrical properties of the transparent electrodes based on percolating networks can be changed by pattern structures. For this study, we photolithographically patterned the three types of materials (graphene, the nanotrough, and the hybrid) with diverse widths (Figure 2a), and then measured their resistances after depositing two contact pads of metals (5 nm thick Cr and 300 nm thick Au). The R_s of each pattern was calculated from the measured resistance (Supporting Information), and Figure 2b indicates the dependence of R_s on the widths of the patterns. Although R_s of the 2D graphene layer showed negligible dependence on the width, its R_s (>1000 Ω/sq) was quite high compared to the ITO case. In contrast to graphene, the R_s of the nanotrough varied significantly when the widths of patterns were changed because the percolating networks of the nanotrough became locally disconnected by the patterning. Although the variation of the nanotrough's R_s was insignificant when the width was greater than ~100 μm, the nanotrough became nonconductive as the width decreased to the threshold level (~100 μm), similar to the open spaces of the nanotrough networks. This dependence of R_s on the geometries of the patterns can cause unwanted, local variations in the resistance of circuits and, therefore, can limit the use of this metal nanotrough for fine and narrow structures of electrodes in compactly integrated circuits. Conversely, the graphene−metal nanotrough hybrid electrode exhibited negligible dependence of R_s on the widths of the patterns, similar to the graphene case, but it also had significantly lower R_s (~1 Ω/sq), even for narrow patterns with widths that were less than 100 μm. For these narrow patterns, the current pathways are formed by the graphene and metal nanotrough in series. The lengths of the metal-line disconnections are typically very short, compared to the overall lengths of the lines, and hence the current pathways connected through the graphene are relatively short and wide. Thus, the high R_s value of graphene does not increase the total resistance of the hybrid patterns significantly. Also, Au composes the nanotrough, and its contact resistance with graphene is relatively low, compared to other metal cases.[41] The hybrid's consistency in R_s and its low resistance are significant advantages.

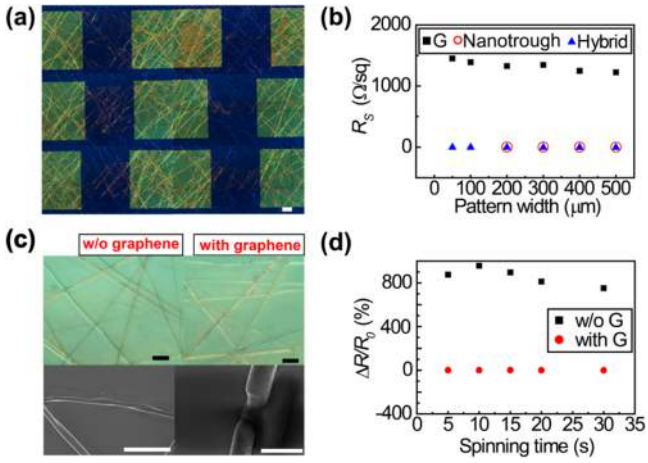

Figure 2. Electrical and thermal properties of the hybrid patterns. (a) Optical micrographs of graphene−metal nanotrough hybrid electrodes with various widths of patterns. White scale bar, 100 μm. (b) Dependence of R_s on the pattern widths of the hybrid (pattern length: 500 μm). (c) Optical micrographs and SEM images of the metal nanotrough or the hybrid under thermal loading (250 °C for 3 h). Black scale bars, 20 μm. White scale bars, 10 μm (left) or 2 μm (right). (d) Relative resistance changes of the nanotrough or the hybrid depending on spinning times.

Compared to the nanotrough only, the hybrid also provided better reliability in maintaining its electric properties under thermal loadings. Figure 2c shows optical micrographs and scanning electron microscope (SEM) images of two different samples, that is, the nanotrough and its hybrid with graphene, after they were heated in air at 250 °C for 3 h. Thin and fine metal lines in the nanotrough networks became partially oxidized or disconnected by melting under thermal loading (left insets in Figure 2c), which resulted in significant increase in the resistance by almost a factor of 800 (Figure 2d). In contrast, the hybrid electrode preserved its resistance (Figure 2d) against thermal loading with negligible oxidation or disconnections of the metal lines (right insets in Figure 2c). This occurred because the graphene that was covering the metal lines acted as a passivation layer, thereby retarding the permeation of oxygen gas and moisture,[42] and it also functioned as a heat sink to spread and dissipate heat.[43]

The hybrid electrode was mechanically flexible and stretchable. As shown in Figure 3a, the hybrid electrodes on a 2 μm thick polyimide substrate were wrapped on various cylindrical supports with different curvatures, and they also were folded in half using tweezers. The right inset shows an SEM image of the folded area (radius of curvature of ~50 μm), and this folding leads to a strain (ε) of 2% in the hybrid[6,14] (Supporting Information). Figure 3b presents the relative changes in resistance as a function of the radius of curvature. No significant change in resistance occurred when the electrodes were bent to radii of curvature as small as 500 μm (ε < 0.2%). Folding the film with 50 μm in the radius (ε = 2%) increased the resistance by about 20%.

Shapes of the collectors used in the electrospinning step can control the alignment of the metal lines in the nanotrough, and their alignment can affect the stretchability of the nanotrough film. For example, ring-type collectors in which the electric field is uniformly circular inside the ring can produce random

dx.doi.org/10.1021/nl502755y | Nano Lett. 2014, 14, 6322−6328

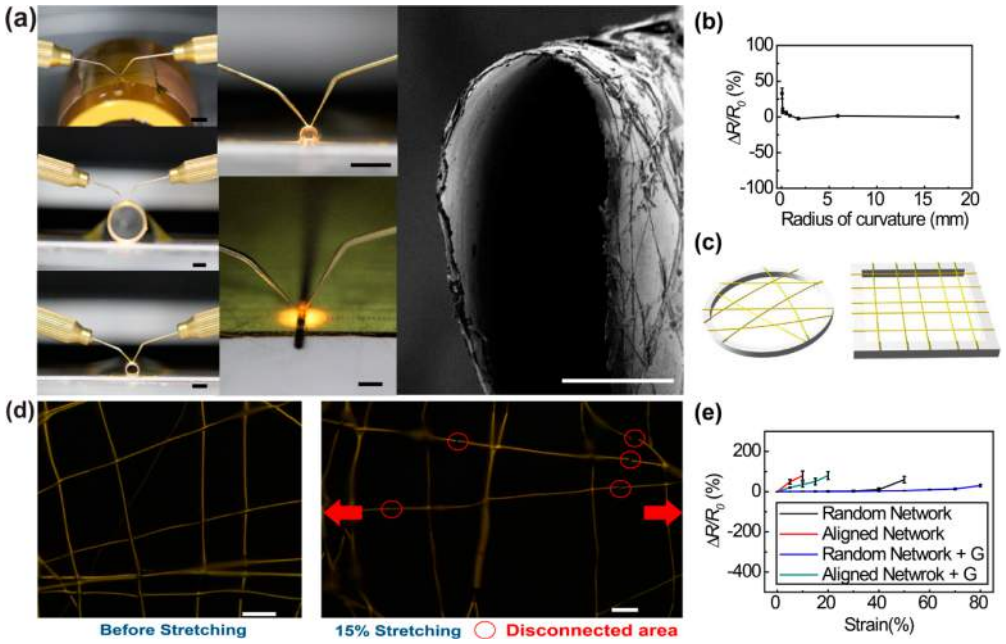

Figure 3. Mechanically flexible and stretchable properties of the hybrid nanostructures. (a) Photographs of the hybrid electrodes wrapped on various cylindrical supports with different curvatures. In the right part of (a) is an SEM image of the hybrid electrode folded in half (radius of curvature: ~50 μm). Black scale bars, 2 mm. White scale bar, 50 μm. (b) Relative resistance changes as a function of the bending radius. (c) Schematic images of the random networks or aligned arrays of free-standing fibers electrospun using ring-type or square-type collectors. (d) Optical micrographs of the aligned metal lines before or after stretching (tensile strain: 15%). Scale bars, 10 μm. (e) Relative resistance changes of the nanotrough or the hybrid as a function of strain.

networks of polymer fibers; square-type collectors in which the field distribution is not uniform inside the square can induce alignment of the fibers (Figure 3c). For the stretchability measurement, these two different metal nanotrough samples (the random networks or aligned arrays of the metal lines) were fabricated on PDMS elastomeric substrates. After clamping these samples by two fixtures connected to the current–voltage measurement system, they were stretched in specific elongation directions and lengths using a mechanical apparatus. When the aligned metal lines (formed using the square-type collector) were stretched parallel to their alignment direction, these metal lines were broken due to the applied tensile force. Figure 3d shows the locally broken parts of the aligned lines that resulted from stretching them into their alignment direction with a 10% strain. After stretching further, the nanotrough with the cracked lines became nonconductive (Figure 3e). However, random networks of the nanotrough can avoid this parallel alignment between the metal lines and stretching direction in most local areas, and this misalignment can dissipate the applied tensile force. For example, the sample of random networks could be stretched up to 50% in strain with an increase in resistance of 60%. Formation of the hybrid graphene–metal nanotrough nanostructures can enhance the stretchability further, because the graphene layer can maintain conductive paths by covering the local disconnections of the metal lines. As presented in Figure 3e, covering the graphene resulted in increases in the maximum tensile strains of the aligned arrays and the random-network samples to of 20 and 80%, respectively. This mechanical stretchability of the hybrid material was superior to that of ITO, which can be cracked by applying a tensile strain of ~1%.

The hybrid graphene–metal nanotrough electrode can be used as source/drain and to interconnect the flexible, transparent, oxide semiconductor thin film transistor (TFT) arrays. Figure 4a shows a photograph and the SEM images of the transistors as well as schematic diagrams of the layouts of the devices. For this demonstration, all components of the device had to be transparent. The fabrication process began by spin-coating of a 2 μm thick, transparent polyimide substrate (Supporting Information Figure 4) on a handling Si wafer on which a 300 nm thick poly(methyl methacrylate) (PMMA) sacrificial layer was precoated. After spinning a suspension of Ag nanowires (AgNWs) on the polyimide, a CVD-synthesized graphene layer was transferred to form the graphene–AgNW hybrid film[30] and then this hybrid film was patterned as gate electrodes using oxygen plasma. A Zr-doped aluminum oxide (ZAO) dielectric layer covered one of the gate electrodes as a high-k material.[44,45] Next, an In_2O_3 semiconducting layer was spun and thermally annealed at 200 °C in air.[46] After patterning the channel dimensions photolithographically, formations of source/drain and interconnects using the graphene–metal nanotrough hybrid completed the fabrication of the TFT arrays. These final devices on the polyimide film could be peeled off of the Si wafer easily by dissolving the PMMA with acetone. All of these transparent components of the devices provided high transmittance (~90%) in the visible light range, as shown in Figure 4b. Figure 4c presents the transfer (left inset) and output (right) characteristics of the TFTs. The graphs indicate typical n-channel behavior. The performances of the 80 TFTs were measured, and their statistical distributions of mobility (μ_{dev}) and threshold voltage (V_{th}) are provided in Figure 4d,e. These data fit Gaussian profiles, and the average values of μ_{dev} and V_{th} in the saturation regime were 125 ± 14 $cm^2/V{\cdot}s$ and 1.0 ± 0.6 V, respectively; in the linear regime, the values were 105 ± 15 $cm^2/V{\cdot}s$ and 1.7 ± 0.9 V, respectively. Also, these TFTs showed a high on/off ratio that exceeded ~10^5. The mobility of these TFTs with the hybrid electrodes was significantly greater than mobility of the

dx.doi.org/10.1021/nl502755y | Nano Lett. 2014, 14, 6322–6328

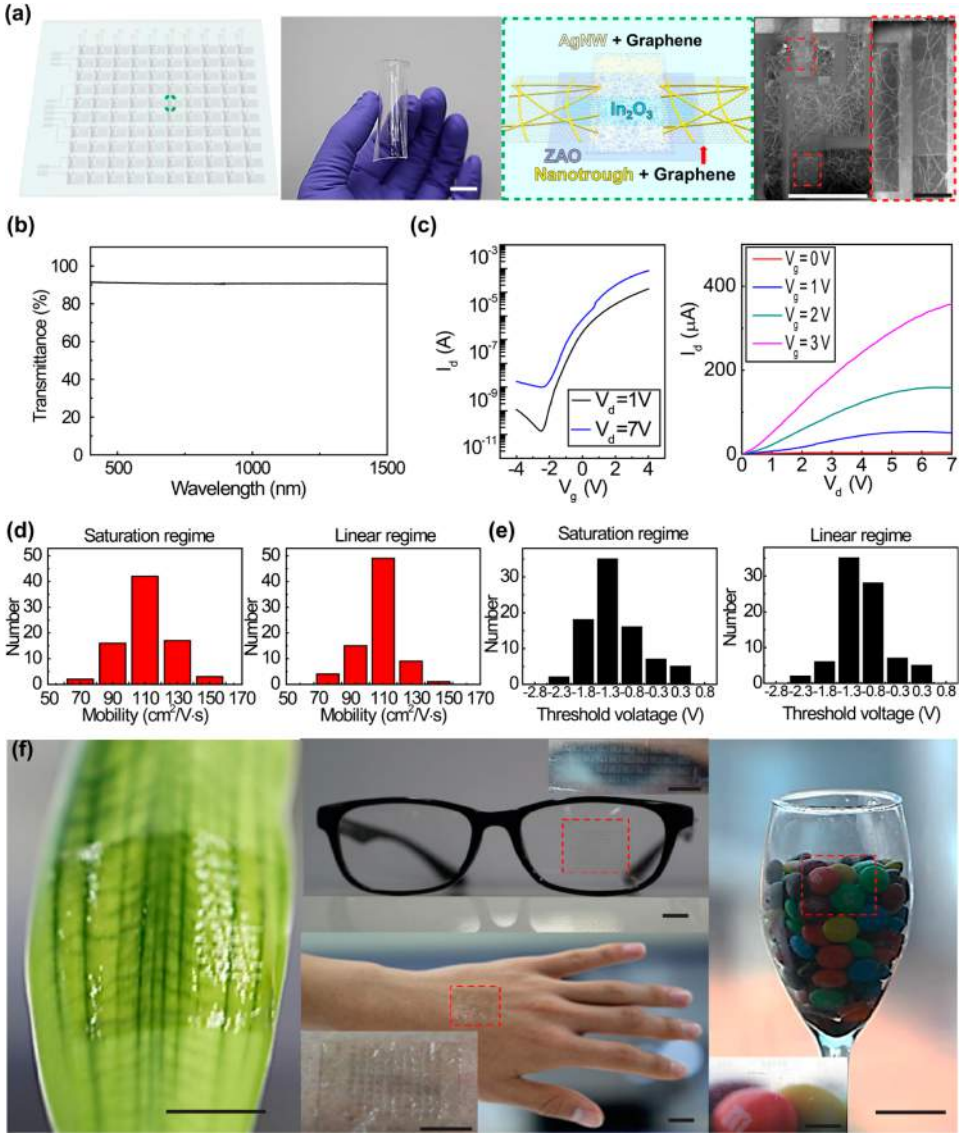

Figure 4. Fabrications of oxide semiconductor TFT arrays using the hybrid electrode as source/drain and interconnects electrodes. (a) A schematic image (left) of the flexible and transparent TFT array. A photo (middle) of the TFT array sample on a transparent polyimide substrate (scale bar; 1 cm). A schematic diagram (middle) of the TFT layout. SEM images (right) of the TFTs (black scale bar, 500 μm; white scale bar, 100 μm). (b) Optical transmittance spectrum of the transparent TFT array. Here transmittance of the polyimide substrate was excluded. (c) Transfer (I_d–V_g, left) and output (I_d–V_d, right) characteristics of the transistor in linear (V_d, 1 V) or saturation (V_d, 7 V) regimes. (d,e) Statistical distributions of mobility and threshold voltage in saturation (left) or linear (right) regimes. (f) Photographs of the TFT arrays transferred on leaf, eyeglasses, a drinking glass, and the skin of human hand. All scale bars are 1 cm.

amorphous Si TFTs (~1 cm^2/V·s), which are used mainly for commercial liquid crystal displays (LCDs) or organic light-emitting displays (OLEDs). The hybrid graphene–metal nanotrough structure could withstand electrical load and enabled stable TFT operations without the electrical breakdown of source/drain and interconnects. Also, the high transparency and flexibility of the hybrid electrodes were advantageous for transparent and flexible TFT arrays. For example, Figure 4f and Supporting Information movie S1 demonstrate the TFT backplane sample attached on various nonplanar surfaces, such as a leaf (*D. sanderiana* cv. Virens, also as known as "lucky bamboo"), eyeglasses, a drinking glass, and the skin of a human hand, suggesting substantial potential for applications in transparent and flexible displays or wearable electronics.

In conclusion, in this paper, we described the advantages of graphene–metal nanotrough hybrid nanostructures as flexible, stretchable, transparent electrodes. The hybridization of two-dimensional graphene and one-dimensional metal nanotrough networks improved the electrical properties of the devices significantly, such as highly uniform R_s, negligible dependence of R_s on pattern geometries, and the ability to maintain very low R_s and high transparency. The hybrid electrodes reliably preserved these properties under thermal loading, and it also had superb mechanical flexibility and stretchability. Compared to previous results on flexible, transparent electrodes, the hybrid structure shows the superb levels of flexibility, transparency, and R_s (Supporting Information Table S1). Thus, these hybrid electrodes can be used to fabricate flexible and transparent oxide semiconductor TFT arrays on various nonplanar surfaces, including leaves, eyeglasses, and human

dx.doi.org/10.1021/nl502755y | *Nano Lett.* 2014, 14, 6322–6328

skin. We believe this approach presents a promising strategy for developing flexible and wearable electronic devices, indicating substantial promise of next-generation electronics.

■ ASSOCIATED CONTENT

Supporting Information

Experimental details of graphene−metal nanotrough hybrid electrode structure, device fabrications, characterization technique, and supporting figures and movies. This material is available free of charge via the Internet at http://pubs.acs.org.

■ AUTHOR INFORMATION

Corresponding Author

*E-mail: jangung@unist.ac.kr.

Author Contributions

B.W.A. designed and performed the experiments, fabricated the devices, and analyzed the data. B.G.H., S.Y.K., M.K., M.S.L., and K.L. contributed to the sample preparations and data analysis. J.B.K, H.Y.C., and B.S.B. advised on the device designs and analyses. J.U.P. oversaw all research phases and revised the manuscript. All authors discussed and commented on the manuscript.

Notes

The authors declare no competing financial interest.

■ ACKNOWLEDGMENTS

This work was supported by the Ministry of Science, ICT & Future Planning and the Ministry of Trade, Industry and Energy of Korea through Basic Science Research Program of National Research Foundation (2013R1A2A2A01068542), IT R&D program (10041416), Materials Original Technology Program (10041222), and Technology Innovation Program (Grant 10044410).

■ REFERENCES

(1) Burroughes, J.; Bradley, D.; Brown, A.; Marks, R.; Mackay, K.; Friend, R.; Burns, P.; Holmes, A. *Nature* **1990**, *347* (6293), 539−541.

(2) Yu, G.; Cao, A.; Lieber, C. M. *Nat. Nanotechnol.* **2007**, *2* (6), 372−377.

(3) Park, J. U.; Meitl, M.; Hur, S. H.; Usrey, M. L.; Strano, M. S.; Kenis, P. J.; Rogers, J. A. *Angew. Chem.* **2006**, *118* (4), 595−599.

(4) Wu, Z.; Chen, Z.; Du, X.; Logan, J. M.; Sippel, J.; Nikolou, M.; Kamaras, K.; Reynolds, J. R.; Tanner, D. B.; Hebard, A. F. *Science* **2004**, *305* (5688), 1273−1276.

(5) Shim, B. S.; Zhu, J.; Jan, E.; Critchley, K.; Kotov, N. A. *ACS Nano* **2010**, *4* (7), 3725−3734.

(6) Park, J.-U.; Nam, S.; Lee, M.-S.; Lieber, C. M. *Nat. Mater.* **2012**, *11* (2), 120−125.

(7) Nair, R.; Blake, P.; Grigorenko, A.; Novoselov, K.; Booth, T.; Stauber, T.; Peres, N.; Geim, A. *Science* **2008**, *320* (5881), 1308−1308.

(8) Chen, J.-H.; Jang, C.; Xiao, S.; Ishigami, M.; Fuhrer, M. S. *Nat. Mater.* **2008**, *3* (4), 206−209.

(9) Emtsev, K. V.; Bostwick, A.; Horn, K.; Jobst, J.; Kellogg, G. L.; Ley, L.; McChesney, J. L.; Ohta, T.; Reshanov, S. A.; Röhrl, J. *Nat. Mater.* **2009**, *8* (3), 203−207.

(10) Reina, A.; Jia, X.; Ho, J.; Nezich, D.; Son, H.; Bulovic, V.; Dresselhaus, M. S.; Kong, J. *Nano Lett.* **2008**, *9* (1), 30−35.

(11) Li, X.; Cai, W.; An, J.; Kim, S.; Nah, J.; Yang, D.; Piner, R.; Velamakanni, A.; Jung, I.; Tutuc, E. *Science* **2009**, *324* (5932), 1312−1314.

(12) Kim, K. S.; Zhao, Y.; Jang, H.; Lee, S. Y.; Kim, J. M.; Kim, K. S.; Ahn, J.-H.; Kim, P.; Choi, J.-Y.; Hong, B. H. *Nature* **2009**, *457* (7230), 706−710.

(13) Li, X.; Zhu, Y.; Cai, W.; Borysiak, M.; Han, B.; Chen, D.; Piner, R. D.; Colombo, L.; Ruoff, R. S. *Nano Lett.* **2009**, *9* (12), 4359−4363.

(14) Bae, S.; Kim, H.; Lee, Y.; Xu, X.; Park, J.-S.; Zheng, Y.; Balakrishnan, J.; Lei, T.; Kim, H. R.; Song, Y. I. *Nat. Nanotechnol.* **2010**, *5* (8), 574−578.

(15) Zhu, Y.; Sun, Z.; Yan, Z.; Jin, Z.; Tour, J. M. *ACS Nano* **2011**, *5* (8), 6472−6479.

(16) Kim, K. K.; Reina, A.; Shi, Y.; Park, H.; Li, L.-J.; Lee, Y. H.; Kong, J. *Nanotechnology* **2010**, *21* (28), 285205.

(17) Lieber, C. M. *MRS Bull.* **2011**, *36* (12), 1052−1063.

(18) Wang, C.; Hu, Y.; Lieber, C. M.; Sun, S. *J. Am. Chem. Soc.* **2008**, *130* (28), 8902−8903.

(19) Wu, Y.; Xiang, J.; Yang, C.; Lu, W.; Lieber, C. M. *Nature* **2004**, *430* (6995), 61−65.

(20) Wang, D.; Lieber, C. M. *Nat. Mater.* **2003**, *2* (6), 355−356.

(21) De, S.; Higgins, T. M.; Lyons, P. E.; Doherty, E. M.; Nirmalraj, P. N.; Blau, W. J.; Boland, J. J.; Coleman, J. N. *ACS Nano* **2009**, *3* (7), 1767−1774.

(22) Hu, L.; Kim, H. S.; Lee, J.-Y.; Peumans, P.; Cui, Y. *ACS Nano* **2010**, *4* (5), 2955−2963.

(23) De, S.; Coleman, J. N. *MRS Bull.* **2011**, *36* (10), 774−781.

(24) Yang, L.; Zhang, T.; Zhou, H.; Price, S. C.; Wiley, B. J.; You, W. *ACS Appl. Mater. Interfaces* **2011**, *3* (10), 4075−4084.

(25) Hu, W.; Niu, X.; Li, L.; Yun, S.; Yu, Z.; Pei, Q. *Nanotechnology* **2012**, *23* (34), 344002.

(26) Hu, L.; Wu, H.; Cui, Y. *MRS Bull.* **2011**, *36* (10), 760−765.

(27) Catrysse, P. B.; Fan, S. *Nano Lett.* **2010**, *10* (8), 2944−2949.

(28) Ahn, S. H.; Guo, L. J. *Nano Lett.* **2010**, *10* (10), 4228−4234.

(29) Wu, H.; Kong, D.; Ruan, Z.; Hsu, P.-C.; Wang, S.; Yu, Z.; Carney, T. J.; Hu, L.; Fan, S.; Cui, Y. *Nat. Nanotechnol.* **2013**, *8* (6), 421−425.

(30) Lee, M.-S.; Lee, K.; Kim, S.-Y.; Lee, H.; Park, J.; Choi, K.-H.; Kim, H.-K.; Kim, D.-G.; Lee, D.-Y.; Nam, S. *Nano Lett.* **2013**, *13* (6), 2814−2821.

(31) Jeong, C.; Nair, P.; Khan, M.; Lundstrom, M.; Alam, M. A. *Nano Lett.* **2011**, *11* (11), 5020−5025.

(32) Kholmanov, I. N.; Stoller, M. D.; Edgeworth, J.; Lee, W. H.; Li, H.; Lee, J.; Barnhart, C.; Potts, J. R.; Piner, R.; Akinwande, D. *ACS Nano* **2012**, *6* (6), 5157−5163.

(33) Peng, H.; Dang, W.; Cao, J.; Chen, Y.; Wu, D.; Zheng, W.; Li, H.; Shen, Z.-X.; Liu, Z. *Nat. Chem.* **2012**, *4* (4), 281−286.

(34) Zhang, M.; Fang, S.; Zakhidov, A. A.; Lee, S. B.; Aliev, A. E.; Williams, C. D.; Atkinson, K. R.; Baughman, R. H. *Science* **2005**, *309* (5738), 1215−1219.

(35) Hecht, D. S.; Hu, L.; Irvin, G. *Adv. Mater.* **2011**, *23* (13), 1482−1513.

(36) Wu, H.; Hu, L.; Rowell, M. W.; Kong, D.; Cha, J. J.; McDonough, J. R.; Zhu, J.; Yang, Y.; McGehee, M. D.; Cui, Y. *Nano Lett.* **2010**, *10* (10), 4242−4248.

(37) Leem, D. S.; Edwards, A.; Faist, M.; Nelson, J.; Bradley, D. D.; de Mello, J. C. *Adv. Mater.* **2011**, *23* (38), 4371−4375.

(38) Ghosh, D.; Martinez, L.; Giurgola, S.; Vergani, P.; Pruneri, V. *Opt. Lett.* **2009**, *34* (3), 325−327.

(39) Lipomi, D. J.; Vosgueritchian, M.; Tee, B. C.; Hellstrom, S. L.; Lee, J. A.; Fox, C. H.; Bao, Z. *Nat. Nanotehcnol.* **2011**, *6* (12), 788−792.

(40) Lee, J.-Y.; Connor, S. T.; Cui, Y.; Peumans, P. *Nano Lett.* **2008**, *8* (2), 689−692.

(41) Song, S. M.; Park, J. K.; Sul, O. J.; Cho, B. J. *Nano Lett.* **2012**, *12* (8), 3887−3892.

(42) Bunch, J. S.; Verbridge, S. S.; Alden, J. S.; van der Zande, A. M.; Parpia, J. M.; Craighead, H. G.; McEuen, P. L. *Nano Lett.* **2008**, *8* (8), 2458−2462.

(43) Balandin, A. A.; Ghosh, S.; Bao, W.; Calizo, I.; Teweldebrhan, D.; Miao, F.; Lau, C. N. *Nano Lett.* **2008**, *8* (3), 902−907.

(44) Jeong, S.; Lee, J.-Y.; Lee, S. S.; Seo, Y.-H.; Kim, S.-Y.; Park, J.-U.; Ryu, B.-H.; Yang, W.; Moon, J.; Choi, Y. *J. Mater. Chem. C* **2013**, *1* (27), 4236−4243.

(45) Yang, W.; Song, K.; Jung, Y.; Jeong, S.; Moon, J. *J. Mater. Chem. C* **2013**, *1* (27), 4275−4282.

(46) Hwang, Y. H.; Seo, J.-S.; Yun, J. M.; Park, H.; Yang, S.; Park, S.-H. K.; Bae, B.-S. *NPG Asia Mater.* **2013**, *5* (4), e45.